ELSEVIER

Journal of Fluids and Structures 23 (2007) 1064–1076

JOURNAL OF FLUIDS AND STRUCTURES

www.elsevier.com/locate/jfs

Vortex shedding from a circular cylinder near a moving wall

Wei-Xi Huang, Hyung Jin Sung*

Department of Mechanical Engineering, Korea Advanced Institute of Science and Technology, 373-1 Guseong-dong, Yuseong-gu, Daejeon 305-701, Korea

Received 3 April 2006; accepted 16 February 2007
Available online 30 April 2007

Abstract

Flow over a circular cylinder near a moving plane wall is simulated numerically. The influence of the moving wall on the vortex shedding from the cylinder is demonstrated and the corresponding mechanism is illustrated using instability theory. A critical gap ratio between the circular cylinder and the moving wall is defined, and a precise method for determining the critical gap ratio is proposed. The drag and lift forces and the pressure coefficient are presented as a function of the gap ratio. The scaling of the Strouhal number is discussed.

Keywords: Circular cylinder; Ground effect; Vortex shedding; Strouhal number

1. Introduction

Understanding the influence of a plane wall on the flow past a vehicle is of fundamental importance in the automobile industry. A simple model of this type of flow is to tow a circular cylinder parallel to a stationary wall with the cylinder axis perpendicular to the wall in an otherwise quiescent ambient fluid. By fixing the coordinate system to the cylinder, this model is equivalent to the system in which the fluid flows over a fixed circular cylinder near a moving wall whose velocity is the same as that of the incoming flow. Under these conditions, no boundary layer is formed on the wall. The presence of the moving wall reduces the flow rate through the gap between the cylinder and wall and forces more fluid to flow over the other side, resulting in a mean lift force that is absent for the isolated cylinder case without the wall. The moving wall inhibits the normal velocity and stabilizes the flow, and suppresses vortex shedding. The main governing parameters are the Reynolds number $\mathrm{Re} = U_\infty D/v$ and the gap ratio G/D, where U_∞ denotes the free-stream velocity, D is the circular cylinder diameter, v is the kinematic viscosity and G denotes the gap height (the shortest distance between the cylinder and wall).

When the wall is stationary relative to the cylinder, a boundary layer is formed on the wall. This makes the problem much more complicated. In this case, the flow is affected not only by the relative thickness δ/D but also by the relative position δ/G (Zdravkovich, 2003), where δ is the boundary layer thickness. Many previous studies have examined this problem in the subcritical regime, i.e., the regime in which the boundary layer along the cylinder surface is laminar until separation (Zdravkovich, 1997). These studies established that when the gap G is less than a certain critical value, vortex shedding is suppressed (Bearman and Zdravkovich, 1978). Previous studies have consistently indicated that this critical

*Corresponding author. Tel.: +82 42 869 3027; fax: +82 42 869 5027.
E-mail address: hjsung@kaist.ac.kr (H.J. Sung).

0889-9746/$ - see front matter © 2007 Elsevier Ltd. All rights reserved.
doi:10.1016/j.jfluidstructs.2007.02.004

gap ratio $(G/D)_C$ is about 0.3, as summarized by Price et al. (2002). However, the mechanism of vortex shedding suppression is still a controversial issue. Grass et al. (1984) and Taniguchi and Miyakoshi (1990) argued that, when the cylinder is close to the wall, vorticity cancellation occurs between the shear layer along the lower cylinder side facing the wall and that along the wall. However, Price et al. (2002) observed that the two shear layers associated with the wall and the lower side of the cylinder do not cancel out. Furthermore, the small flow rate through the gap and the existence of a mean shear stress in the boundary layer along the wall are also the factors contributing to the suppression of vortex shedding (Zdravkovich, 2003; Bhattacharyya and Maiti, 2004; Bhattacharyya et al., 2006).

In vehicle aerodynamics, the moving wall condition has to be considered in some situations, such as flows over a road wheel (Bearman, 1980) and ground effect type racing cars (Katz, 2006). However, only a small number of studies have examined the flow over a bluff body near a moving wall. Taneda (1965) carried out an experiment in a water tunnel by towing a circular cylinder parallel to a wall at a low Reynolds number (Re = 170) and observed that a single vortex row is formed behind the cylinder at the gap ratio $G/D = 0.1$. Kumarasamy and Barlow (1997) solved the flow over a half cylinder close to a moving wall by Reynolds-averaged Navier–Stokes (N–S) simulations and compared the results to those obtained for the stationary wall case. They found that the kinematic condition of the wall does not affect the gross flow characteristics, such as the Strouhal number and lift force, but does significantly alter the trajectory of the vortices behind the cylinder. Bhattacharyya and Maiti (2005) simulated the two-dimensional laminar flow past a square cylinder placed parallel to a moving wall; they found that vortex shedding occurs even at the very small gap ratio of $G/D = 0.1$.

In the present study, we carried out numerical simulations of flow over a circular cylinder near a moving wall. For real flow cases, three-dimensionality of vortex shedding from an isolated cylinder begins to develop at about Re = 194 (Williamson, 1996). Although Bailey et al. (2002) found that the vortex formation process is increasingly two-dimensional when the gap ratio is less than about 0.7, the flow is not guaranteed to be two-dimensional for all Reynolds numbers (ranging from 200 to 600) and gap ratios (ranging from 0.1 to ∞) considered in the present simulations. On the other hand, as pointed out by Perry et al. (1982), the two-dimensional patterns of vortex shedding from a bluff body have the same qualitative features as those of the fully turbulent phase-averaged results. Based on the above discussion, in this paper we assume the flow to be two-dimensional and focus on the variations of the vortex shedding scenario under the ground effect and discuss its mechanism. The variations of the forces and shedding frequencies are also presented. In the next section, we introduce the numerical methods and carefully validate the present simulations. The results and discussion are presented in Section 3, and conclusions are drawn in Section 4.

2. Numerical methods and validation

We consider the flow over a circular cylinder located above a wall that is moving at the same velocity as the free-stream velocity. The governing equations are the unsteady incompressible N–S equations and the continuity equation. In the present work, we solve the governing equations in a Cartesian grid system and the immersed boundary method is employed to simulate the solid surface of the circular cylinder (Kim et al., 2001). The governing equations are

$$\frac{\partial \vec{u}}{\partial t} + \left(\vec{u}\cdot\nabla\right)\vec{u} = -\nabla p + \frac{1}{\mathrm{Re}}\nabla^2\vec{u} + \vec{f}, \tag{1}$$

$$\nabla\cdot\vec{u} - q = 0, \tag{2}$$

where $\vec{u} = (u, v)$ is the velocity vector, p is the pressure, $\vec{f} = (f_x, f_y)$ is the momentum forcing applied to enforce the no-slip boundary conditions along the immersed boundary, i.e., the cylinder surface and q is the mass source/sink term added to the continuity equation to satisfy the mass conservation for the grid cells cut by the immersed boundary.

The N–S equations are solved by the fractional step method on a staggered Cartesian grid. The velocity components and momentum forcings are defined on the staggered grid, whereas the pressure and the mass source/sink term are applied at the centre of the cell. Details regarding the N–S solver can be found in Kim et al. (2002). The interpolation schemes of the immersed boundary method for calculating the momentum forcings f_x and f_y are taken from Kim et al. (2001). An accurate formulation of the mass source/sink term proposed by Huang and Sung (2007) is used.

Fig. 1 shows a schematic diagram of the present computational configuration and the coordinate system. The x and y coordinates are fixed on the circular cylinder. The origin is located on the wall for all cases except the case of an isolated cylinder without a wall, for which the origin is located at the centre of the cylinder.

To validate the present numerical method, the flow over an isolated circular cylinder without a wall is simulated and the results are compared with those of previous studies. The computational domain is a rectangle surrounding the

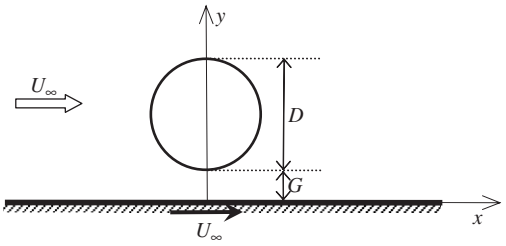

Fig. 1. Schematic diagram of the computational configuration and coordinate system.

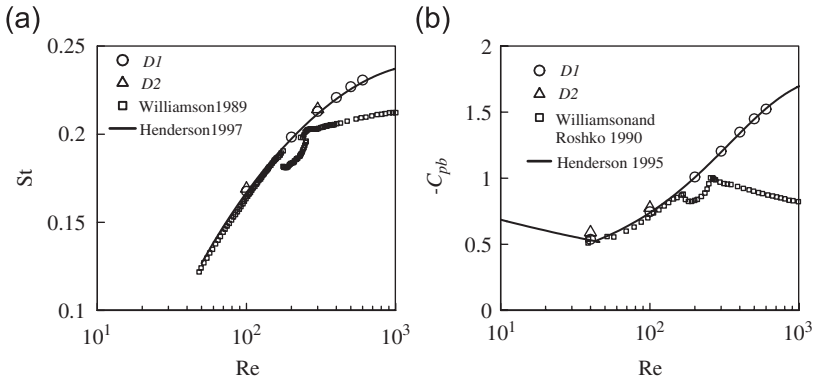

Fig. 2. (a) Strouhal number and (b) base pressure coefficient for the flow past an isolated cylinder in freestream.

cylinder. Two domain sizes are selected for comparison. The larger one (referred to as D1) extends from $-15D$ upstream of the cylinder to $35D$ downstream of the cylinder along the streamwise direction, and extends from $-15D$ to $15D$ in the normal direction, with the origin at the centre of the cylinder. The grid dimensions used for D1 are 501×451 in the streamwise and normal directions, respectively. The grid is uniformly distributed inside the cylinder and stretched outside the cylinder. The smaller domain (D2) has the same size in the streamwise direction as D1 and a smaller size in the normal direction, extending from $-10D$ to $10D$. The grid dimensions of D2 are 257×151. A Dirichlet boundary condition ($u = U_\infty,\ v = 0$) is employed at the inlet and far-field boundaries, and a convective boundary condition is used at the outlet boundary. The no-slip boundary condition on the cylinder surface is satisfied by momentum forcing in Eq. (1). Fig. 2 shows the Strouhal number and base pressure coefficient obtained from the simulations in both domains. The results of D1 agree well with previous numerical simulations (Henderson, 1995, 1997) and experimental measurements in the two-dimensional regime (Williamson, 1989; Williamson and Roshko, 1990), while those of D2 show a slight deviation. Hence, we use the domain D1 in the present study. Next the validation is extended to the flow over a circular cylinder confined between two parallel walls. The domain ranges from $-7.5D$ to $17.5D$ in the streamwise direction and the walls are located at $y = \pm 2.5D$. The cylinder is located at the origin. The grid size is 257×151. Fig. 3 shows a good agreement between the present result and that of Zovatto and Pedrizzetti (2001).

When the circular cylinder is close to a moving wall, the computational domain extends from the wall ($y = 0$) to the top boundary ($y = L_y = 15D$) in the normal direction, and the domain size in the streamwise direction is the same as that of D1. For the case of a cylinder located very near to the wall, the grid resolution in the gap must be fine if we are to obtain accurate data. This makes the simulation computationally more expensive than the isolated cylinder case. For the smallest gap considered in the present simulation ($G = 0.1D$), a grid refinement test is performed at $\mathrm{Re} = 300$. Note that when the cylinder is located close to a wall, the flow is stabilized and the critical Reynolds number for periodic vortex shedding is increased significantly. In the present simulation, when the gap ratio G/D is 0.1, the periodic vortex shedding is decaying at $\mathrm{Re} = 200$ and is only sustained when $\mathrm{Re} \geqslant 300$. The grid dimensions of the coarse, medium and fine grid systems tested are 417×251, 513×301 and 641×401, respectively. The grid number in the normal direction inside the gap is 8, 10 and 16 for the three grid systems, respectively. The mean drag and lift coefficients and Strouhal number values for the three grid systems are very close for the three systems (summarized in Table 1). Fig. 4 shows the profiles of the streamwise and normal mean velocity in the gap. The streamwise mean velocity profiles for both the coarse and medium grid systems agree well with that obtained using the fine grid (Fig. 4(a)). However, the normal mean

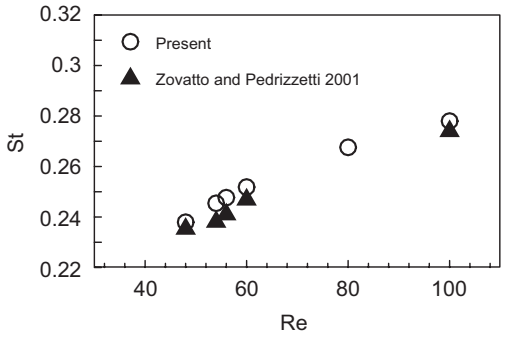

Fig. 3. Strouhal number for the flow past a circular cylinder confined between parallel walls.

Table 1
Comparison of the drag coefficient, the lift coefficient and the Strouhal number among three grid systems for $G/D = 0.1$ at $\mathrm{Re} = 300$

Grid number	C_D	C_L	St
Coarse	1.614	0.794	0.128
Medium	1.611	0.792	0.128
Fine	1.611	0.790	0.128

velocity profile for the coarse grid system shows slightly less accurate prediction than the profiles obtained using the medium and fine grids (Fig. 4(b)) due to its small magnitude. Accordingly, we use the medium grid system in the present study. For $G<0.5D$, the grid is uniformly distributed inside both the cylinder and the gap but was stretched above the cylinder in the normal direction. For $G\geqslant 0.5D$, by contrast, the grid was uniformly distributed inside the cylinder but stretched inside the gap and above the cylinder.

3. Results and discussion

3.1. Vortex shedding

Figs. 5–8 show the instantaneous vorticity contours near the cylinder and the time histories of the drag and lift forces (denoted by C_d and C_l, respectively) for $D/G = 0$, 5/3, 5 and 10 at $\mathrm{Re} = 300$. Instead of using the parameter G/D (the gap ratio), we use its inverse, D/G, so that the cases of small gap height can be represented more clearly and the isolated cylinder case without a wall ($D/G = 0$) can be included easily in all figures in the present paper. D/G increases as the cylinder moves toward the wall. For the case of the isolated cylinder without a wall (i.e., $D/G = 0$), Fig. 5(a) shows the vorticity contours at four instants (denoted by A, B, C and D, respectively) in a shedding cycle; the corresponding points are marked in the time history of the drag coefficient shown in Fig. 5(b). Symmetric alternating shedding vortices are observed behind the cylinder. Both the drag and lift forces vary periodically with time, with the former having a frequency twice that of the latter. The vortex shedding from the upper side of the cylinder, at instant A, results in the maximum drag force and the minimum lift force, while the vortex shedding from the lower side, at instant C, results in the maximum drag force and the maximum lift force.

For $D/G = 5/3$, pairs of vortices are shed from the cylinder alternately and the shear layers with opposite sign of the vortices appear on the wall (Fig. 6(a)). However, the vortex formed at the lower side of the cylinder matures early and is shed from the cylinder in a short time, resulting in a small local maximum value of the drag force, as indicated by the instants B and C in Fig. 6(b).

For a larger value of $D/G = 5$, the vortices from both sides of the cylinder are no longer shed alternately (Fig. 7(a)). Instead, the lower side vortex is shed immediately following the upper side one and then the vortex pair leaves the cylinder together. Correspondingly, the drag coefficient and the lift coefficient vary at the same frequency, as shown in Fig. 7(b).

For $D/G = 10$, the shear layer along the lower side of the cylinder and the shear layer along the wall downstream are incorporated and roll up together (Fig. 8(a)). The gap flow rate becomes so small that the time required to form a vortex

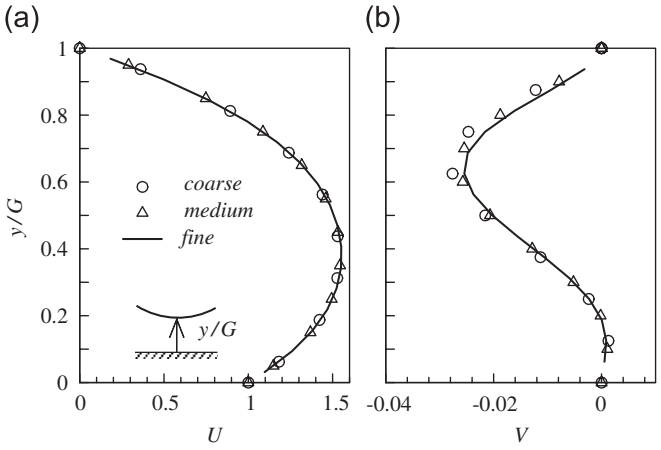

Fig. 4. Mean flow velocity in the gap for $G/D = 0.1$ at $\mathrm{Re} = 300$: (a) streamwise velocity; (b) normal velocity. Three grid systems (coarse, medium and fine) are compared, which have 8, 10 and 16 grids, respectively, inside the gap.

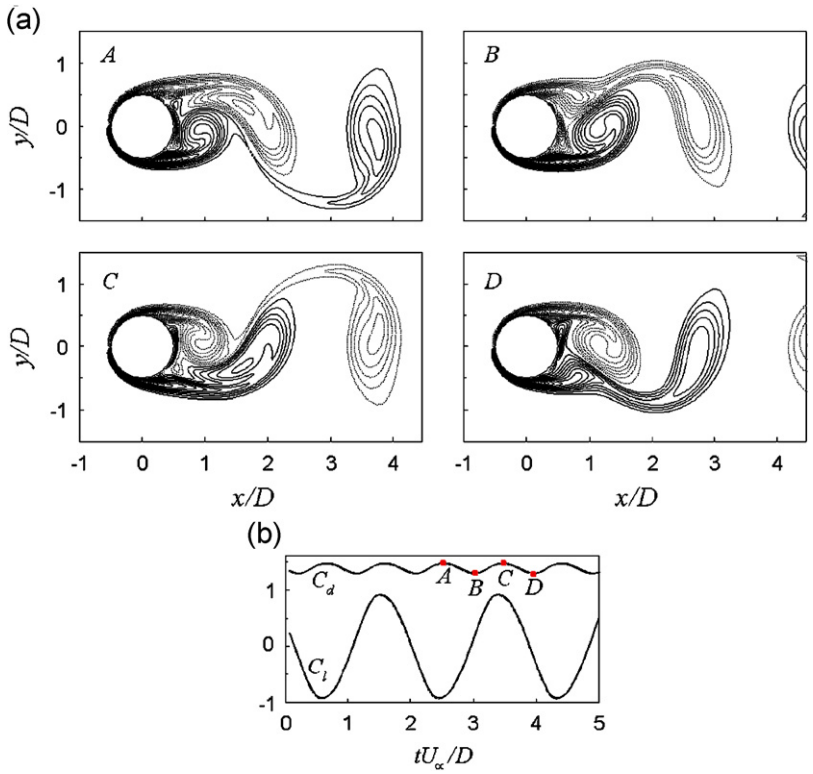

Fig. 5. Scenario of vortex shedding for $D/G = 0$ at $\mathrm{Re} = 300$: (a) instantaneous vorticity contour; (b) time history of drag coefficient and lift coefficient.

at the lower side of the cylinder increases substantially, resulting in a flat peak in the drag coefficient from instant A to B, as shown in Fig. 8(b). The vortex pair from the two sides of the cylinder is shed together and the drag and lift coefficients vary at the same frequency. Due to the dominance of the upper side vortex, the present results are consistent with the experimental finding of Taneda (1965) that a single vortex row forms behind a cylinder at this gap height.

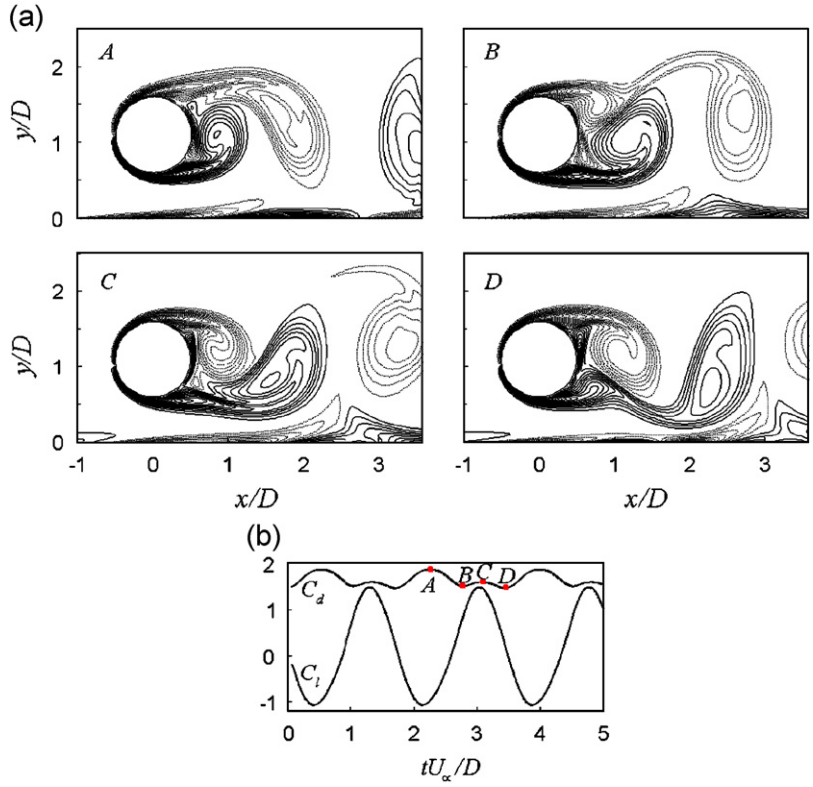

Fig. 6. Scenario of vortex shedding for $D/G = 5/3$ at $\mathrm{Re} = 300$: (a) instantaneous vorticity contour; (b) time history of drag coefficient and lift coefficient.

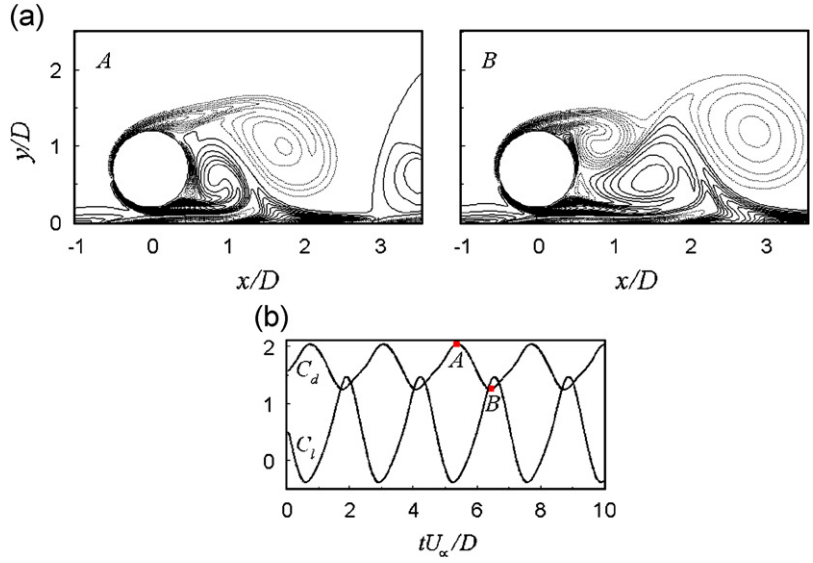

Fig. 7. Scenario of vortex shedding for $D/G = 5$ at $\mathrm{Re} = 300$: (a) instantaneous vorticity contour; (b) time history of drag coefficient and lift coefficient.

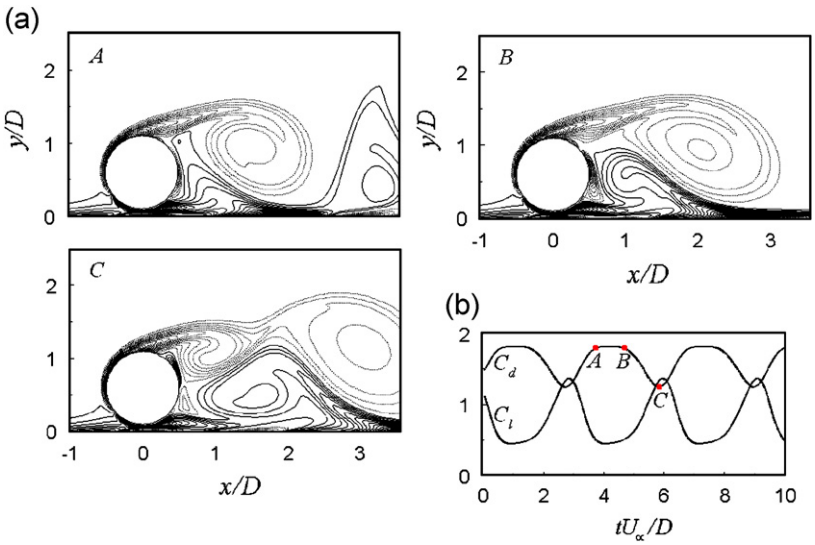

Fig. 8. Scenario of vortex shedding for $D/G = 10$ at $\mathrm{Re} = 300$: (a) instantaneous vorticity contour; (b) time history of drag coefficient and lift coefficient.

3.2. Mean velocity profile in the gap

The mechanism underlying the ground effect can be related to the mean velocity profile in the gap. Fig. 9 shows the streamwise mean velocity U for the inverse gap ratios $D/G = 0$, 5/3, 5 and 10 at $\mathrm{Re} = 300$. The y coordinate is normalized by the gap height (G), such that it ranges from $y/G = 0$ at the wall to $y/G = 1$ at the cylinder. For the isolated cylinder case (i.e., $D/G = 0$), the velocity abruptly increases from zero to its maximum under the cylinder surface and then decreases to the velocity of the far field at about $y/G = 0.8$. The velocity profile contains an inflection point, which is a necessary condition for instability according to Rayleigh's theorem (Drazin and Reid, 1981). It is easy to verify that Fjørtoft's condition is also satisfied (Drazin and Reid, 1981), i.e., $U''(U - U_S) < 0$ somewhere in the mean velocity profile, where U'' denotes the second derivative of U and U_S denotes the mean velocity at the inflection point. For $D/G = 5/3$, the flow is accelerated in the gap. Two local maximum points are observed in the velocity profile, as well as two inflection points. For $D/G = 5$ and 10, however, the profile contains only one local maximum and no inflection point is observed, indicating that the velocity profile is stable according to Rayleigh's and Fjørtoft's theorems. Together with Figs. 5–8, it is obvious that the stability property of the mean velocity profile at the gap is consistent with the status of vortex shedding from the lower side of the cylinder.

In the present study, we can define the critical gap ratio $(G/D)_C$ at which alternating vortex shedding disappears and the shear layer along the lower side of the cylinder rolls up in an entirely passive manner, induced by the upper side vortices. This is equivalent to the critical value at which the mean velocity profile in the gap becomes stable according to the instability analysis. Its inverse is denoted by $(D/G)_C$. Fig. 10 shows the maximum value of the mean streamwise velocity in the gap and the positions of the maxima as a function of D/G. Below $D/G = 3.6$, there are two maximum points, whereas only one maximum point appears above $D/G = 3.6$. This is consistent with the profiles in Fig. 9, in which the inflection point disappears above $D/G = 3.6$, indicating a critical value. Note that this critical value, which corresponds to $G/D = 0.28$, agrees well with previously reported values of the critical gap ratio for the stationary wall case (about 0.3). In addition, in a study of the flow past a square cylinder near a stationary wall, Kim et al. (2005) observed a strong correlation between the periodic vortex shedding mechanism and the position of the maximum mean velocity in the gap. Specifically, they found that as the position of the maximum velocity approaches the lower surface of the cylinder, regular vortex shedding occurs. It is obvious that their observation agrees with the present results. Kumarasamy and Barlow (1997) found that the critical gap ratio is affected little by the kinematic condition of the wall. Thus the stability mechanism may explain the suppression of vortex shedding for the stationary wall case, while in the moving wall case, the vortex at the lower side of the cylinder is formed due to the larger gap flow rate.

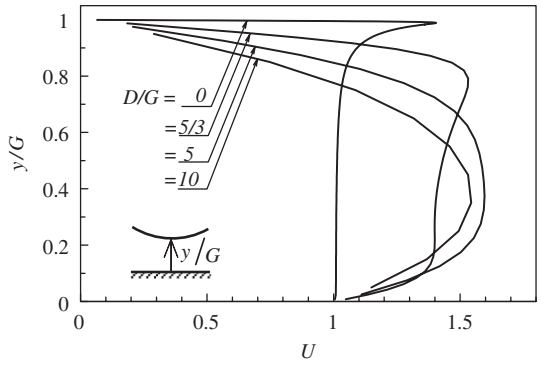

Fig. 9. Streamwise mean velocity in the gap for $D/G = 0$, 5/3, 5 and 10 at $\mathrm{Re} = 300$.

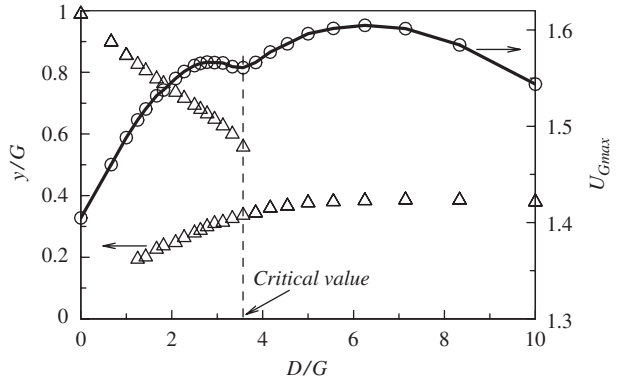

Fig. 10. The maximum value and its position of the streamwise mean velocity in the gap as a function of D/G at $\mathrm{Re} = 300$.

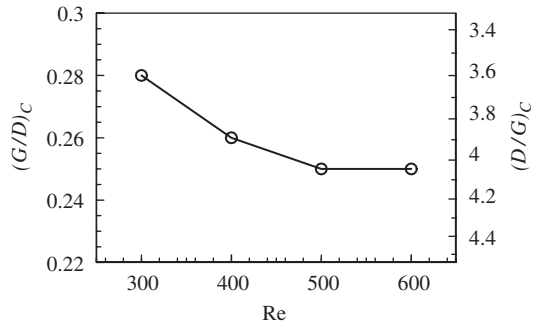

Fig. 11. Critical gap ratio at different Reynolds numbers.

An interesting feature to note in Fig. 10 is that between the two local maxima of the maximum value of the mean gap flow, there is a local minimum point corresponding to the critical value (about $D/G = 3.6$). This feature can assist in the precise determination of the critical value. As pointed out by Lei et al. (1999), it is difficult to accurately determine the critical gap ratio, because experiments and numerical simulations are typically carried out only at certain discrete gap ratios while the alternating vortex shedding disappears gradually as the gap ratio is reduced. The power spectrum of the signal of velocity fluctuations or lift force cannot give a precise value. Lei et al. (1999) proposed a better method based on the variations of the root-mean-square of the fluctuation of lift coefficient (C'_L); however, the critical value obtained by this method is also not definite. Fig. 11 shows the critical gap ratio determined using the present method as a

function of the Reynolds number. Both $(G/D)_C$ and $(D/G)_C$ are shown in the y direction to facilitate comparison with data from previous studies. The critical gap ratio $(G/D)_C$ decreases with increasing Reynolds number and becomes independent of Reynolds number for $\mathrm{Re} > 500$. At higher Reynolds numbers, the boundary layers formed along the cylinder surface and on the wall under the cylinder become much thinner than the gap height; as a result, the critical gap ratio can be determined by the solution of the potential flow through the gap and thus is independent of the Reynolds number.

3.3. Drag and lift forces

The drag and lift coefficients are defined as follows:

$$C_d = \frac{F_x}{\frac{1}{2}\rho U_\infty^2 D}, \quad C_l = \frac{F_y}{\frac{1}{2}\rho U_\infty^2 D}, \tag{3,4}$$

where F_x and F_y denote the total forces exerted on the cylinder by the fluid in the streamwise and normal directions, respectively, due to the pressure and shear stress distributions. Since the grid does not conform to the cylinder surface, it is not a trivial problem to calculate the shear stress along the cylinder surface. Lai and Peskin (2000) provided a useful discussion on this issue and proposed that the forces exerted on the cylinder are equal to the negative of the momentum forcing applied by the boundary to the fluid according to Newton's third law of motion. Thus the forces are calculated easily by integrating the momentum forcings f_x and f_y which have already been obtained after solving Eq. (1). i.e.,

$$F_x = -\int_\Omega f_x \,\mathrm{d}x\,\mathrm{d}y \quad \text{and} \quad F_y = -\int_\Omega f_y \,\mathrm{d}x\,\mathrm{d}y, \tag{5}$$

where Ω is the computational domain.

Fig. 12 shows the mean drag and lift coefficients (denoted by C_D and C_L, respectively) as a function of D/G. In addition to $\mathrm{Re} = 300$, results at other Reynolds numbers ranging from 200 to 500 are also presented for comparison. As shown in Fig. 12(a), the drag coefficient increases with Reynolds number for the same gap height. As the cylinder approaches the wall, the mean drag force increases up to a maximum value at the critical gap ratio $(D/G)_C$, and then decreases with further increases of D/G. In Fig. 12(b), we can see that the lift increases with increasing D/G and decreases with increasing Reynolds number. Interestingly, the lift increases linearly with D/G when $D/G > (D/G)_C$.

Fig. 13 shows the root-mean-squares of the fluctuations of the drag and lift forces (denoted by C'_D and C'_L, respectively) as functions of D/G. As D/G is increased, C'_D increases slightly up to $D/G = 5/3$, then increases rapidly in the range $5/3 < D/G < (D/G)_C$, and subsequently decreases for $D/G > (D/G)_C$ (Fig. 13(a)). C'_L, by contrast, increases as D/G increases for $D/G < 5/3$ and decreases for $D/G > (D/G)_C$, but changes little in the range $5/3 < D/G < (D/G)_C$ (Fig. 13(b)). These variations in C'_D and C'_L are consistent with the vortex shedding scenario under the ground effect. In general, the flow can be characterized by three regions, i.e., large, intermediate and small gaps. The large gap is defined as $D/G < 5/3$ where alternating vortex shedding occurs behind the circular cylinder and the moving wall has little effect on it, the small gap is $D/G > (D/G)_C$ where the vortex shedding from the lower side of the cylinder is entirely passive and dominated by the vortex shedding from the upper side, and the intermediate gap is $5/3 < D/G < (D/G)_C$.

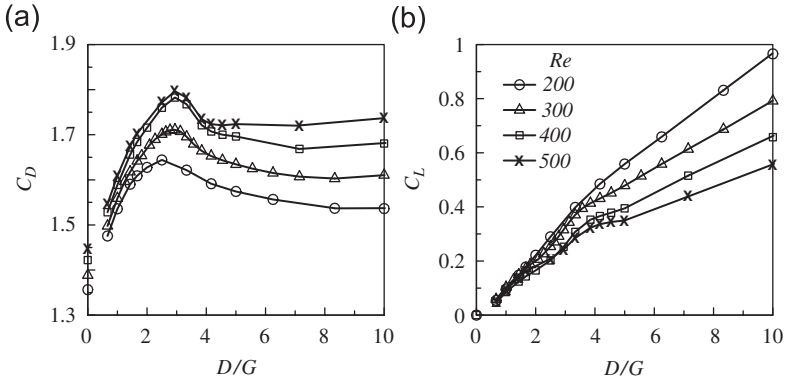

Fig. 12. (a) Mean drag coefficient and (b) mean lift coefficient at $\mathrm{Re} = 200$, 300, 400 and 500.

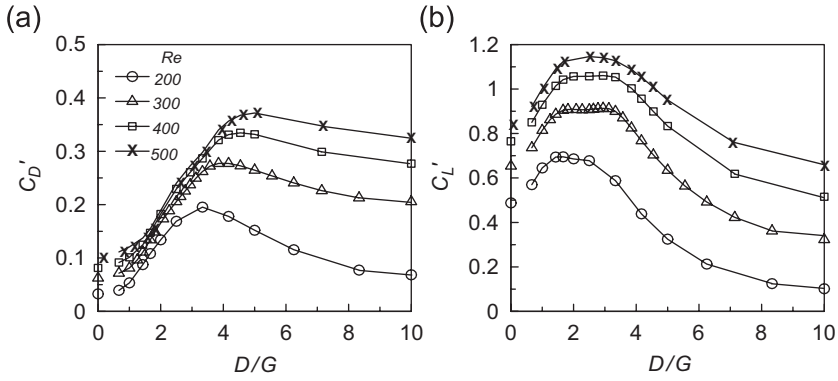

Fig. 13. Root-mean-squares of fluctuations of (a) drag coefficient and (b) lift coefficient at Re = 200, 300, 400 and 500.

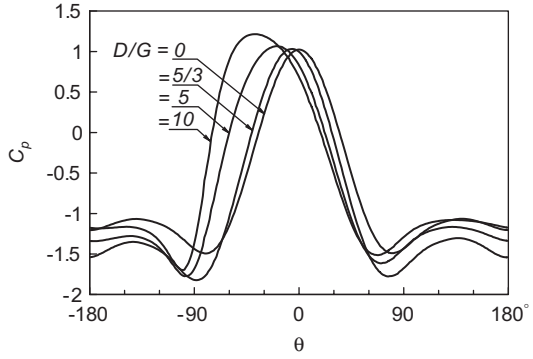

Fig. 14. Pressure coefficient for $D/G = 0,\ 5/3,\ 5$ and 10 at Re = 300.

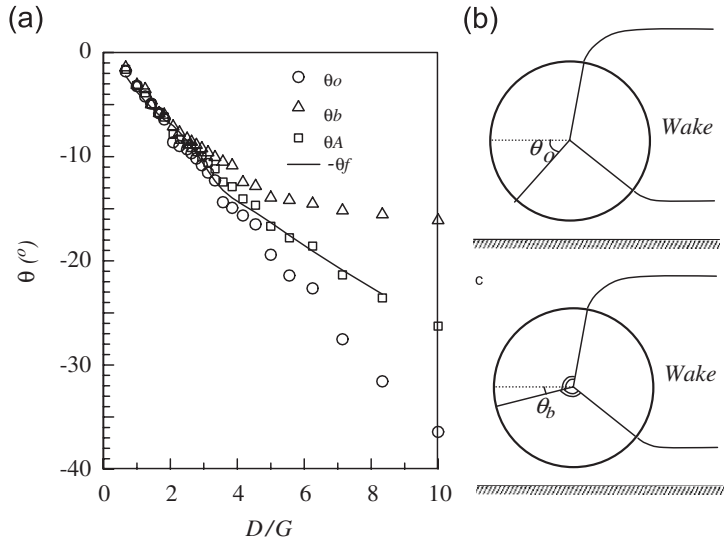

Fig. 15. (a) Comparison of various angles:$-\theta_f$, minus force angle; θ_0, angular position of the front stagnation point; θ_b, angular position of the bisector of the upper- and lower side separation points and $\theta_A = (\theta_0 + \theta_b)/2$; (b) schematic of θ_0; (c) schematic of θ_b.

3.4. Pressure coefficient

The pressure coefficient along the cylinder surface is defined by

$$C_p = \frac{p - p_\infty}{\frac{1}{2}\rho U_\infty^2}, \tag{6}$$

where p_∞ is the pressure at infinity. Fig. 14 shows C_p for $D/G = 0$, 5/3, 5 and 10 at $\mathrm{Re} = 300$. The angle θ is zero at the front point of the horizontal diameter of the cylinder and is counted in the counterclockwise direction, ranging from -180° to 180°. For $D/G = 0$, C_p is symmetric about $\theta = 0$. The lower side and upper side minimum pressure points are located near $\theta = \pm 90^\circ$, respectively. As D/G increases, C_p is skewed to the side of negative angle and the lower side minimum point moves downstream while the upper side one moves upstream.

It is known that the displacement of the front stagnation point contributes mainly to the generation of the mean lift force. In a study on the flow past two cylinders in a side-by-side arrangement, Bearman and Wadcock (1973) found that the rotation of the force vector is fairly consistent with the displacement of the front stagnation point. The force angle is defined as $\theta_f = \tan^{-1}(C_L/C_D)$. The angular position of the front stagnation point θ_0 (see Fig. 15(b)) is determined by the position of the maximum pressure coefficient (Fig. 14). It is also likely that the asymmetry of the two separation points about the front stagnation point due to their displacement also contributes to the forces. This can be represented by the bisector of the angular positions of the upper side and lower side separation points, as shown in Fig. 15(c). The angle of the bisector, denoted by θ_b, is obtained approximately by averaging the angular positions of the two minimum pressure points, as shown in Fig. 14. Fig. 15(a) shows a comparison of $-\theta_f$ with θ_0, θ_b and their average $\theta_A = (\theta_0 + \theta_b)/2$. We find that both θ_0 and θ_b agree well with $-\theta_f$ for $D/G < (D/G)_C$. However, for $D/G > (D/G)_C$, θ_0 decreases faster than $-\theta_f$ as D/G increases, whereas θ_b varies more slowly. Interestingly, the average θ_A agrees well with $-\theta_f$, indicating that the lift force is generated through the combined effect of the displacement of the front stagnation point and the two separation points.

Fig. 16 shows the negative of the base pressure coefficient C_{pb}, which is defined as the pressure coefficient at $\theta = 180^\circ$. Similarly to the mean drag force, $-C_{pb}$ increases as D/G increases for $D/G < (D/G)_C$ and then decreases for $D/G > (D/G)_C$. In addition, for the same gap ratio, $-C_{pb}$ increases with increasing Reynolds number.

3.5. Strouhal number

The Strouhal number is defined as

$$\mathrm{St} = fU_\infty/D, \tag{7}$$

where f is the vortex shedding frequency. St is displayed in Fig. 17(a) as a function of D/G for Reynolds numbers ranging from 200 to 500. St increases with increasing Reynolds number at the same gap ratio, similar to the case of the isolated cylinder without a wall. For $D/G < 5/3$, St increases with increasing D/G due to the acceleration of the gap flow as the cylinder approaches the wall. Then, St decreases rapidly in the range $5/3 < D/G < (D/G)_C$, due to the stabilization effect of the wall. For $D/G > (D/G)_C$, St decreases relatively slowly since the pattern of vortex shedding has been altered.

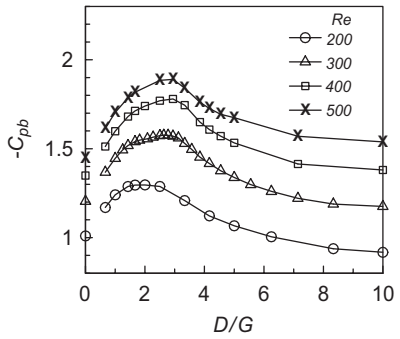

Fig. 16. Base pressure coefficient at $\mathrm{Re} = 200$, 300, 400 and 500.

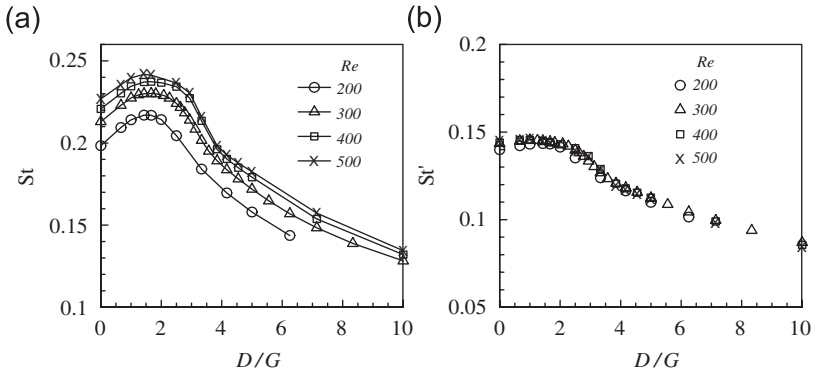

Fig. 17. Strouhal number defined in terms of (a) the free-stream velocity and (b) the separation velocity at Re = 200, 300, 400 and 500.

In terms of the separation velocity (Roshko, 1954),

$$U_S = (1 - C_{pb})^{1/2} U_\infty, \tag{8}$$

the Strouhal number can be defined as

$$\mathrm{St}' = f U_S / D. \tag{9}$$

As shown in Fig. 17(b), St′ collapses into a single curve for different Reynolds numbers. Physically, U_S is the potential flow velocity at the separation point obtained by assuming that the pressure is constant on the rear of the cylinder surface between two separation points. This assumption is valid because of the small variation of C_p after separation (see Fig. 14). Thus U_S denotes the velocity at which the shear layer along the cylinder surface rolls up to form a vortex. As a result, U_S is a better velocity scale than U_∞ to define the Strouhal number for the present asymmetric flow over a circular cylinder.

4. Conclusions

In the present study, a two-dimensional flow over a circular cylinder near a moving wall has been studied numerically. In this system, the kinematic condition of the wall caused the gap flow rate to be much larger than that of the stationary wall. Thus vortex shedding was observed even for small gap distances, in contrast to the behaviour observed for the stationary wall case. However, the vortex shedding from the lower side of the cylinder synchronizes with that from the upper side as the cylinder approaches the wall. The intrinsic mechanism underlying the suppression of the alternating vortex shedding was explained using inviscid instability theory. The stability of the mean velocity profile in the gap is consistent with the status of vortex shedding from the lower side of the cylinder. The stability mechanism may also explain the suppression of vortex shedding for the stationary wall case.

The critical gap ratio $(G/D)_C$ is defined as the gap ratio at which the alternating vortex shedding disappears and the shear layer along the lower side of the cylinder rolls up in an entirely passive manner. The present results indicate that the critical gap ratio corresponds to a local minimum (versus D/G) of the streamwise maximum mean velocity in the gap. Using this feature, the critical gap ratio could be determined precisely. The critical gap ratio decreases with increasing Reynolds number and becomes constant for $\mathrm{Re} > 500$. The variations of the drag and lift forces with Re and D/G were presented. It was shown that the flow can be characterized by three regions, i.e., large gap ($D/G < 5/3$), intermediate gap ($5/3 < D/G < (D/G)_C$) and small gap ($D/G > (D/G)_C$). Interestingly, the rotation of the force vector agreed well with the average of the displacement of the front stagnation point and the bisector of the two separation points. The selection of the velocity scale in the definition of the Strouhal number was discussed. The Strouhal number collapsed into a single curve for different Reynolds numbers when it was defined in terms of the separation velocity.

References

Bailey, S.C.C., Martinuzzi, R.J., Kopp, G.A., 2002. The effects of wall proximity on vortex shedding from a square cylinder: three-dimensional effects. Physics of Fluids 14 (12), 4160–4176.

Bearman, P.W., 1980. Review—bluff body flows applicable to vehicle aerodynamics. ASME Journal of Fluids Engineering 102, 265–274.

Bearman, P.W., Wadcock, A.J., 1973. The interaction between a pair of circular cylinders normal to a stream. Journal of Fluid Mechanics 61, 499–511.

Bearman, P.W., Zdravkovich, M.M., 1978. Flow around a circular cylinder near a plane boundary. Journal of Fluid Mechanics 89, 33–47.

Bhattacharyya, S., Maiti, D.K., 2004. Shear flow past a square cylinder near a wall. International Journal for Engineering Science 42, 2119–2134.

Bhattacharyya, S., Maiti, D.K., 2005. Vortex shedding from a square cylinder in presence of a moving wall. International Journal for Numerical Methods in Fluids 48, 985–1000.

Bhattacharyya, S., Maiti, D.K., Dhinakaran, S., 2006. Influence of buoyancy on vortex shedding and heat transfer from a square cylinder in proximity to a wall. Numerical Heat Transfer, Part A 50, 585–606.

Drazin, P.G., Reid, W.H., 1981. Hydrodynamic Stability. Cambridge University Press, Cambridge.

Grass, A.J., Raven, P.W., Stuart, R.J., Bray, J.A., 1984. The influence of boundary layer velocity gradients and bed proximity on vortex shedding from free spanning pipelines. ASME Journal of Energy Resources Technology 106, 70–78.

Henderson, R.D., 1995. Details of the drag curve near the onset of vortex shedding. Physics of Fluids 7 (9), 2102–2104.

Henderson, R.D., 1997. Nonlinear dynamics and pattern formation in turbulent wake transition. Journal of Fluid Mechanics 352, 65–112.

Huang, W.-X., Sung, H.J., 2007. Improvement of mass source/sink for an immersed boundary method. International Journal for Numerical Methods in Fluids 53, 1659–1671.

Katz, J., 2006. Aerodynamics of race cars. Annual Review of Fluid Mechanics 38, 27–63.

Kim, J., Kim, D., Choi, H., 2001. An immersed-boundary finite-volume method for simulations of flow in complex geometries. Journal of Computational Physics 171, 132–150.

Kim, K., Baek, S.-J., Sung, H.J., 2002. An implicit velocity decoupling procedure for incompressible Navier–Stokes equations. International Journal for Numerical Methods in Fluids 38, 125–138.

Kim, T.-Y., Lee, B.-S., Lee, D.-H., 2005. Study on the unsteady wakes past a square cylinder near a wall. Journal of Mechanical Science and Technology (KSME International Journal) 19 (5), 1169–1181.

Kumarasamy, S., Barlow, J.B., 1997. Computation of unsteady flow over a half-cylinder close to a moving wall. Journal of Wind Engineering and Industrial Aerodynamics 69-71, 239–248.

Lai, M.-C., Peskin, C., 2000. An immersed boundary method with formal second-order accuracy and reduced numerical viscosity. Journal of Computational Physics 160, 705–719.

Lei, C., Cheng, L., Kavanagh, K., 1999. Re-examination of the effect of a plane boundary on force and vortex shedding of a circular cylinder. Journal of Wind Engineering and Industrial Aerodynamics 80, 263–286.

Perry, A.E., Chong, M.S., Lim, T.T., 1982. The vortex-shedding process behind two-dimensional bluff bodies. Journal of Fluid Mechanics 116, 77–90.

Price, S.J., Sumner, D., Smith, J.G., Leong, K., Paidoussis, M.P., 2002. Flow visualization around a circular cylinder near to a plane wall. Journal of Fluids and Structures 16 (2), 175–191.

Roshko, A., 1954. On the drag and shedding frequency of two-dimensional bluff bodies. NACA TN 3169.

Taneda, S., 1965. Experimental investigation of vortex streets. Journal of the Physical Society of Japan 20 (9), 1714–1721.

Taniguchi, S., Miyakoshi, K., 1990. Fluctuating fluid forces acting on a circular cylinder and interference with a plane wall. Experiments in Fluids 9, 197–204.

Williamson, C.H.K., 1989. Oblique and parallel modes of vortex shedding in the wake of circular cylinder at low Reynolds numbers. Journal of Fluid Mechanics 206, 579–627.

Williamson, C.H.K., 1996. Vortex dynamics in the cylinder wake. Annual Review of Fluid Mechanics 28, 477–539.

Williamson, C.H.K., Roshko, A., 1990. Measurements of base pressure in the wake of a cylinder at low Reynolds numbers. Zeitschrift fuer Flugwissenschaften und Weltraumforschung 14, 38–46.

Zdravkovich, M.M., 1997. Flow around circular cylinders, Volume 1. Oxford University Press, Oxford.

Zdravkovich, M.M., 2003. Flow Around Circular Cylinders, vol. 2. Oxford University Press, Oxford.

Zovatto, L., Pedrizzetti, G., 2001. Flow about a circular cylinder between parallel walls. Journal of Fluid Mechanics 440, 1–25.